

# Spike density distribution for the Gierer-Meinhardt model with precursor

Theodore Kolokolnikov\* and Shuangquan Xie†

\**Department of Mathematics and Statistics, Dalhousie University, Halifax, Canada and*

†*Advanced Institute for Materials Research Mathematical Science, Tohoku University, Japan*

We consider the Gierer-Meinhardt model in one dimension with a spatially-dependent precursor  $\mu(x)$ . Assuming that the activator diffuses much slower than the inhibitor, such a system is well-known to admit solutions where the activator concentrates at  $N$  “spikes”. In the large- $N$  limit, we derive the effective spike density for an arbitrary  $\mu(x)$ . We show that this density satisfies a first-order separable ODE. As a consequence, we derive instability thresholds for  $N$  spikes that correspond to a singularity in the ODE for the density. We recover, as a special case, the well-known stability thresholds for constant  $\mu$  first derived in [1], as well as cluster solutions that concentrate near the minimum of  $\mu(x)$  that were recently discovered in [2]. The main trick is applying Taylor expansions and geometric series to the equations of effective spike dynamics.

## 1. INTRODUCTION

The goal of this paper is to characterize the large-scale pattern density in the Gierer-Meinhardt (GM) model with a spatially-variable precursor. GM model is among the simplest reaction-diffusion systems that manifests complex patterns. We study the following version of the GM model [1–3],

$$\varepsilon^2 u_t = \varepsilon^2 u_{xx} - \mu(x)u + u^2/v, \quad 0 = Dv_{xx} - v + \frac{u^2}{\varepsilon} \quad (1.1a)$$

Here,  $u$  and  $v$  represent activator and inhibitor concentrations, respectively, and we make the standard assumption that the inhibitor diffuses much faster than the activator, that is  $\varepsilon^2 \ll D$ . In this case, a pattern forms consisting of a sequence of  $N$  “spikes”, which correspond to localized concentrations of the activator (such as shown in Figure 1). The use of non-constant precursor  $\mu(x)$  was suggested in the original work of Gierer and Meinhardt [3] as a way to model cell differentiation and control pattern distribution in space.

For reasons that will become clear below, we shall assume the following scaling for  $D$  :

$$D = \frac{d^2}{N^2}, \quad d \leq O(1), \quad \text{with } \varepsilon \ll O\left(\frac{d}{N}\right), \quad N \gg O(1). \quad (1.1b)$$

In the case of a constant  $\mu$ , spike patterns have been subject to intensive study over the last two decades, and by now there is a large literature about the formation and stability of these patterns. We refer the reader to books

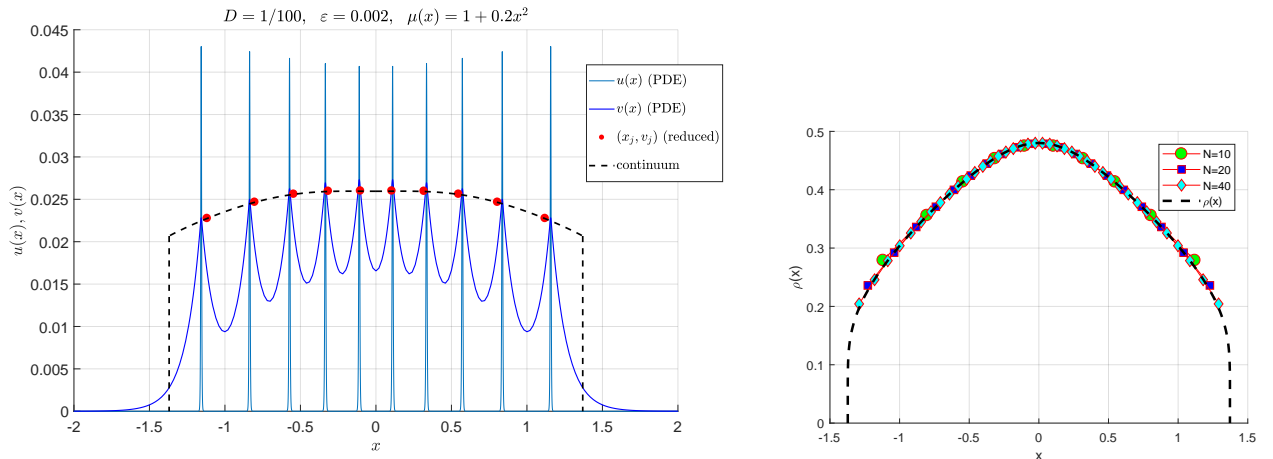


FIG. 1. LEFT: Cluster equilibrium of (1.1) on all of  $\mathbb{R}$  consisting of  $N = 10$  spikes. Red points show the steady state of the reduced system (1.4) for spike positions and weights. Dashed line shows the envelope for  $v(x_j)$  derived from the continuum limit, as well as continuum cluster boundaries. Here,  $N = 10$ ,  $\mu(x) = 1 + 0.2x^2$ ,  $d = 1$ ,  $\varepsilon = 0.002$ . RIGHT: Convergence of spike positions  $x_j$  to the continuum spike density limit  $\rho(x)$  as given by Main Result 2.1. For interior points approximation  $\rho(x) \sim 2d/N/(x_{j+1} - x_{j-1})$  was used; density at endpoints was computed using linear extrapolation of interior points. The points  $x_j$  were computed by running the reduced system (1.4) until equilibrium was reached.

[4, 5] and references therein. One of the most important results goes back to [1]. There, the authors showed that for constant  $\mu$ ,  $N$  spikes on a domain of length  $2L$  are stable as long as

$$\varepsilon \ll d < \frac{L}{\log(1 + \sqrt{2})}. \quad (1.2)$$

When the inequality is reversed, some of the spikes are absorbed by others – so called competition or coarsening instability.

The case of non-constant precursor  $\mu(x)$  was recently studied in [2, 6]. It was found in [2] that for sufficiently small  $d$  (of order  $\varepsilon \ll d \ll O(1)$ ),  $N$  spikes form a *localized cluster* with all  $N$  spikes concentrating near the minimum of  $\mu(x)$ . The spike density within such a cluster was assumed to be (asymptotically) uniform and furthermore, such a cluster was shown to be stable, because  $d$  was taken to be very small.

In contrast to results from [2], the spike cluster that forms when  $d = O(1)$  does *not* have nearly constant density, and is  $O(1)$  in size, rather than being localized at the critical point of  $\mu(x)$ . Our main insight is to derive the continuum limit of the density and spike heights, in the limit  $N \gg 1$ . To give away the punchline, we show that the spike density satisfies the first order separable ODE

$$\frac{d\rho}{dx} = \frac{\mu'(x)}{\mu(x)} \frac{3\rho^3 \sinh(1/\rho) - \frac{5}{2}\rho^2 \sinh^2(1/\rho)}{\cosh(1/\rho) - 3}. \quad (1.3a)$$

Here,  $\rho(x)$  is the continuum limit of spike density, suitably rescaled, and is well approximated by

$$\rho(x) \sim \frac{d}{(x_{k+1} - x_k)N} \quad \text{for } N \gg 1, \quad (1.3b)$$

where  $x_k$  are equilibrium spike locations sorted in increasing order, and  $x$  is close to  $x_k$ .

The inhibitor heights are approximated in terms of density by

$$v(x_k) \sim \frac{12N}{d} \tanh\left(\frac{1}{2\rho(x_k)}\right) \mu^{-3/2}(x_k). \quad (1.3c)$$

Figure 1 illustrates our result, showing an  $O(1)$  cluster of 10 spikes. The dashed line shows our continuum prediction for the spike height envelope as well as cluster boundaries, in excellent agreement with the full PDE simulation.

Based on our continuum density formulation, we explicitly compute a threshold  $d_{\max}$  such that the spike cluster ceases to exist when  $d$  is gradually increased above  $d_{\max}$ . In this case, spike coarsening is observed. See Figure 2 for an example.

We also show that if the domain size is sufficiently large (or equivalently, if  $\mu'(x)$  is sufficiently small), there is a *secondary* threshold  $d_c$ , with  $d_c < d_{\max}$ , which predicts the cluster formation. Namely, for  $d < d_c$ , the spike cluster has compact support inside the domain, whereas for  $d_c < d < d_{\max}$  the spike cluster spans the entire cluster. This is illustrated in Figure 1.

As a starting point, we use by-now-standard techniques to reduce the full PDE solution on an infinite domain to an ODE system for spike positions  $x_j$  coupled to spike weights  $v_j$ . The derivation is rather standard [1, 2, 5–7], and is relegated to Appendix A. The resulting reduced system is:

$$\frac{d}{dt} x_k = -2\mu^{1/2}(x_k) \left( \frac{\langle v_x \rangle_k}{v_k} + \frac{5}{4} \frac{\mu'(x_k)}{\mu(x_k)} \right), \quad (1.4a)$$

$$v_k = \sum_{j=1}^N S_j \frac{N}{2d} e^{-|x_k - x_j| \frac{N}{d}}, \quad \langle v_x \rangle_k = \sum_{j=1}^N S_j \frac{N^2}{2d^2} e^{-|x_k - x_j| \frac{N}{d}} \text{sign}(x_j - x_k) \quad (1.4b)$$

$$S_k = 6\mu^{3/2}(x_k) v_k^2 \quad (1.4c)$$

with the convention that  $\text{sign} 0 = 0$ . Here,  $x_k$  is the location of the center of the spike  $k$ , and  $v_k$  is the height of the inhibitor at  $x_k$ :

$$v_k \sim v(x_k, t) \quad (1.5a)$$

whereas the activator is approximated by  $N$  localized  $\text{sech}^2$ -type spikes:

$$u(x, t) \sim \sum_{j=1}^N v_j \mu(x_j) \frac{3}{2} \text{sech}^2\left(\frac{x - x_j}{2\varepsilon \mu^{-1/2}(x_j)}\right). \quad (1.5b)$$

The steady state solution then satisfies

$$0 = \frac{-2}{\eta_k} \sum_{j \neq k} C_j \frac{N}{2d} e^{-|x_k - x_j|N/d} \text{sign}(x_j - x_k) - \frac{5}{2} \frac{\mu'(x_k)}{\mu(x_k)} \quad (1.6a)$$

$$\eta_k = \sum_j \frac{1}{2} e^{-|x_k - x_j|N/d} C_j, \quad \text{where } C_j = \eta_j^2 \mu_j^{3/2}; \quad \eta_j = \frac{6N}{d} v_j. \quad (1.6b)$$

## 2. CONTINUUM LIMIT

We now derive the continuum limit of equations (1.6). Under the scaling (1.1b), the spike cluster density will be shown to be proportional to  $N$ , so that the inter-spike distance scales like  $1/N$ . With this in mind, suppose  $s \in [0, 1]$  and define  $x(s)$  such that

$$x_j = x\left(\frac{j}{N}\right), \quad j = 1 \dots N. \quad (2.7)$$

Now consider the spikes in the interior of the cluster, that is,  $1 \ll k \ll N$ . Let  $s = k/N$  and define

$$x = x(s), \quad r := \exp(-x'(s)/d) \quad \text{where } s = k/N. \quad (2.8)$$

A key idea is to use Taylor series and geometric series. The key computation is the following estimate:

$$\begin{aligned} \sum_j \frac{1}{2} e^{-|x_k - x_j|N/d} C_j &\sim \sum_{l=-\infty}^{\infty} \frac{1}{2} e^{-\frac{x'}{d}|l|} C\left(x + \frac{l}{N}x'\right) \\ &\sim \frac{C(x)}{2} \sum_{l=-\infty}^{\infty} r^{-|l|} \\ &\sim \frac{C}{2} \frac{1+r}{1-r}. \end{aligned} \quad (2.9)$$

Similarly, we estimate

$$\begin{aligned} \sum_{j \neq k} C_j N \frac{1}{2d} e^{-|x_k - x_j|N/d} \text{sign}(x_j - x_k) &\sim -\frac{C}{2d^2} x'' \sum_{l=0}^{\infty} e^{-\frac{x'}{d}l} l^2 + \frac{C_x x'}{d} \sum_{l=0}^{\infty} e^{-\frac{x'}{d}l} l \\ &\sim -x'' \frac{C}{2d^2} \frac{r^2 + r}{(1-r)^3} + \frac{C_x x'}{2d} \frac{2r}{(1-r)^2} \end{aligned} \quad (2.10)$$

Therefore the expressions (1.6) simplify to

$$0 = \frac{-2}{\eta} \left( -x'' \frac{C}{2d^2} \frac{r^2 + r}{(1-r)^3} + \frac{C_x x'}{2d} \frac{2r}{(1-r)^2} \right) - \frac{5}{2} \frac{\mu'(x_k)}{\mu(x_k)} \quad (2.11)$$

$$\eta = \frac{C}{2} \frac{1+r}{1-r}, \quad C = \eta^2 \mu^{3/2}. \quad (2.12)$$

We now define the *density* to be

$$\rho := \frac{d}{x'(s)}. \quad (2.13)$$

For finite but large  $N$ , equation (1.3b) is just the finite-difference approximation of (2.13).

We compute,

$$\frac{dx}{ds} = \frac{d}{\rho}; \quad \frac{d^2x}{ds^2} = -d^2 \frac{\rho_x}{\rho^3}.$$

Equations (2.11, 2.12) then become

$$\eta = 2 \frac{1-r}{1+r} \mu^{-3/2}, \quad C = 4 \left( \frac{1-r}{1+r} \right)^2 \mu^{-3/2}, \quad r = e^{-1/\rho}, \quad (2.14)$$

$$0 = -\frac{1}{\eta} \left( \frac{\rho_x}{\rho^3} C \frac{r^2+r}{(1-r)^3} + C_x \frac{1}{\rho} \frac{2r}{(1-r)^2} \right) - \frac{5}{2} \frac{\mu'(x_k)}{\mu(x_k)} \quad (2.15)$$

Eliminating  $C$  and  $\eta$ , after some algebra, we obtain the **continuum limit equations** (1.3), which is the main result of this paper.

An additional constraint on the density comes from mass constraint. Suppose that the density is compactly supported on the interval  $[a, b]$ , so that  $x_1 \rightarrow a$  and  $x_N \rightarrow b$ . Then

$$\int_a^b \rho dx = d \int_0^1 ds = d. \quad (2.16)$$

We now consider two cases: either the domain is all of  $\mathbb{R}$  or the domain is finite. Let's consider the infinite domain first. In this case, we claim that the density  $\rho(x)$  decays to zero at the boundaries of the cluster:  $\rho(x) \rightarrow 0$  as  $x \rightarrow a^+$  or  $x \rightarrow b^-$ . To see this, take  $k = 1$  in (1.6) and estimate:

$$\sum_j \frac{1}{2} e^{-|x_1-x_j|N/d} C_j \sim \frac{1}{2} \frac{1}{1-r} C(a) \sim \eta(a); \quad (2.17)$$

$$\sum_{j \neq 1} C_j \frac{N}{2d} e^{-|x_1-x_j|N/d} \text{sign}(x_j - x_1) \sim C(a) \frac{N}{2d} \left( \frac{1}{1-r} - 1 \right) \sim -\eta(a) \frac{5}{2} \frac{\mu'(a)}{\mu(a)}. \quad (2.18)$$

where  $r = e^{-d/\rho(a)}$ . Combining (2.17) and (2.18) yields

$$e^{-d/\rho(a)} \sim -\frac{5d}{N} \frac{\mu'(a)}{\mu(a)} \rightarrow 0 \text{ as } N \rightarrow \infty$$

which shows that the density decays to zero at the boundaries. Therefore we obtain the following result

**Main Result 2.1** *Consider the steady-state of the GM system (1.1) consisting of  $N$  spikes on all of  $\mathbb{R}$ . In the limit  $N \gg 1$ , the spike density satisfies the first-order separable ODE (1.3a), subject to the conditions*

$$\int_a^b \rho(x) dx = d, \quad \rho(a) = 0 = \rho(b); \quad \rho(x) \geq 0 \text{ for } x \in [a, b]. \quad (2.19)$$

*The envelope for spike heights satisfies (1.3c).*

**Example.** Take  $\mu(x) = 1 + 0.2x^2$ ,  $d = 1$ . Because  $\mu$  is even, we have  $a = -b$ , so we let  $[a, b] = [-l, l]$  and conditions (2.19) are equivalent to

$$\rho(l) = 0, \quad \int_0^l \rho(x) dx = d/2. \quad (2.20)$$

We then solve the ODE (1.3a) numerically starting with  $\rho(0) = \rho_0$  and adjusting  $\rho_0$  until (2.20) are satisfied. In this way, we find that  $l \approx 1.4$  and  $\rho(0) \approx 0.47$ . This is illustrated in Figure 2 (top left). Figure 1 shows continuum density distribution, and comparison with reduced dynamics for spike centers as well as the full PDE simulation. Excellent agreement is observed.

**Stability threshold and maximum spike density.** Figure 2 (top left) shows the solution to the ODE (1.3a) with  $\mu(x) = 1 + 0.2x^2$ , and for several choices of  $\rho_0 = \rho(0)$ . Note that the denominator on the right hand side of (1.3a) is zero when  $\cosh(1/\rho) - 3 = 0$ . This is the maximum admissible value of  $\rho$ . We therefore define

$$\rho_{\max} := \frac{1}{\text{arccosh}(3)} = 0.5673. \quad (2.21)$$

When  $\rho_0 = \rho_{\max}$ , a ‘‘corner’’ is visible in this figure (due to the fact that  $\mu'(0) = 0$ ). When  $\rho(0) > \rho_{\max}$ , it is easy to show that the density blows up and is therefore inadmissible. Therefore we must have  $0 < \rho < \rho_{\max}$ . It is easy to show that  $l$  as well as the total mass  $d = 2 \int_0^l \rho(x) dx$  is an increasing function of  $\rho_0$ . Therefore the maximum possible value of  $d$  is attained by setting  $\rho(0) = \rho_{\max}$ . Call the corresponding value of  $d$ ,  $d_{\max}$ . The steady state breaks down if  $d$  is gradually increased past  $d_{\max}$ .

We now summarize this result.

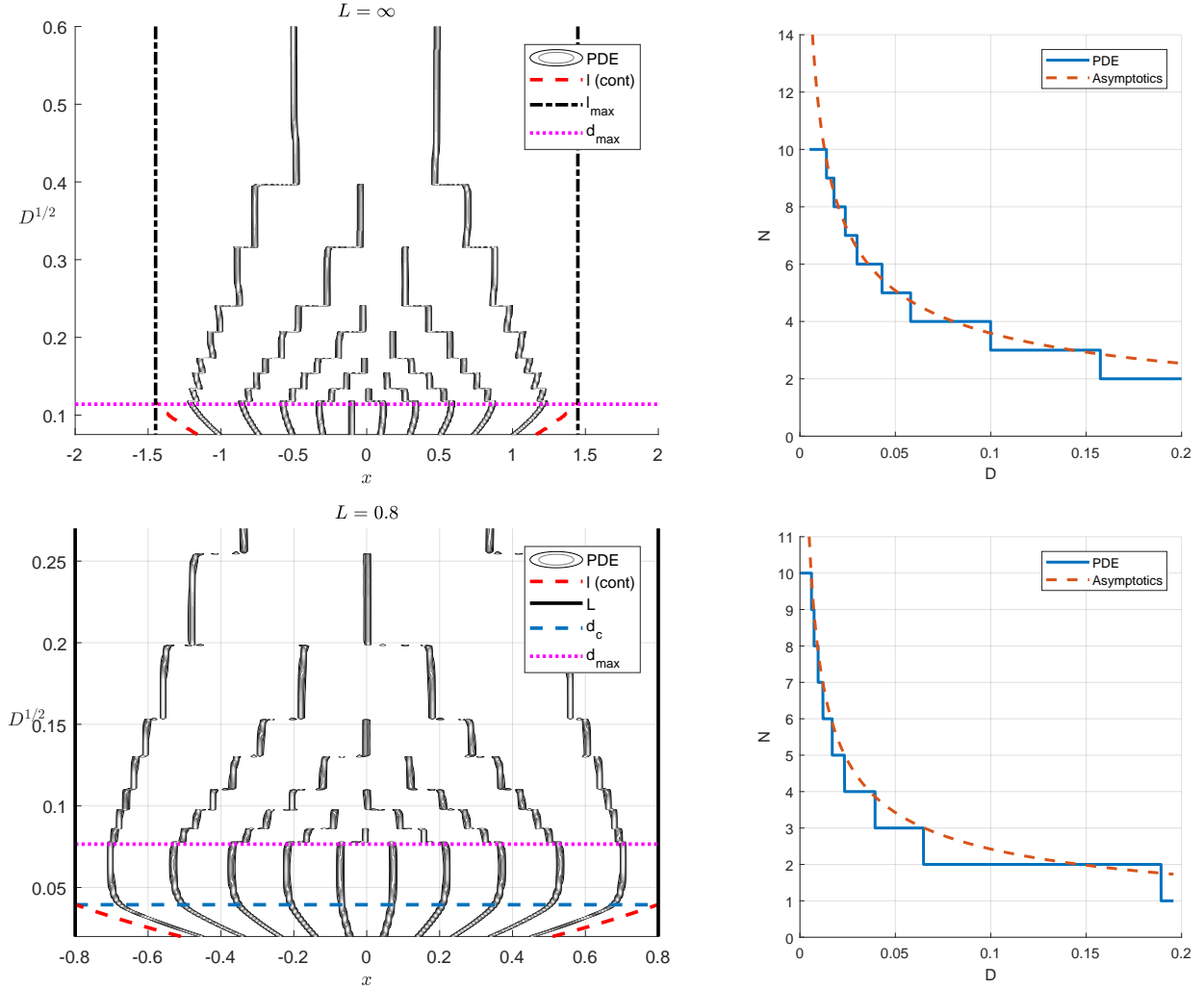


FIG. 2. Top row: simulation of (1.1) on a large domain (top left). Initial conditions consist of 10 spikes with  $D$  increasing gradually according to the formula  $D = 0.001 + 10^{-6}t$  with  $\varepsilon = 0.005$  and  $\mu(x) = 1 + 0.2x^2$ . Continuum spike density support is indicated by dashed line. It has a maximum radius of  $l_{\max} = 1.448$  corresponding to  $d = d_{\max} = 1.14$ . Spike coarsening is predicted whenever  $N = d_{\max}/\sqrt{D}$  (as plotted on the vertical scale); this is in good agreement with full numerics, as shown on top right. Bottom left: Simulation of (1.1) on the finite domain  $[-L, L]$  with  $L = 0.8$  and the same  $\mu(x)$ . Since  $L < l_{\max}$ , the spike cluster first expands to fill up the whole domain without any coarsening event. The interior cluster forms when  $d < d_c = 0.39$ , but the steady state exists for a wider range  $d < d_{\max} = 0.766$  and becomes unstable as  $d$  is increased above  $d_{\max}$ . Bottom right shows excellent agreement with full numerics.

**Main Result 2.2** Suppose  $\mu(x)$  has a minimum at  $x = x_0$ . Let  $\rho(x)$  be the solution to (1.3a) with  $\rho(x_0) = \rho_{\max} = \frac{1}{\operatorname{arccosh}(3)} \approx 0.5673$ , and let  $d_{\max}$  be the corresponding  $d$  as given by (2.19). Then the spike cluster solution exists when  $d < d_{\max}$  and disappears when  $d > d_{\max}$ .

To illustrate this result, consider again  $\mu(x) = 1 + 0.2x^2$ . We find that  $d_{\max} = 1.1364$  with  $-a = b = l_{\max} = 1.45$ . When  $D$  is gradually increased,  $d$  is eventually increased past  $d_{\max}$ , triggering a competition instability which results in spike death. This in turn *decreases*  $d$  slightly below  $d_{\max}$  and the process repeats. In other words,  $N$  spikes exist provided that  $N < 1.1364/\sqrt{D}$ , and the cluster is compactly supported on an interval  $[-l_{\max}, l_{\max}]$ . Refer to Figure 2 (top row), which shows an excellent agreement with full numerical simulations of (1.1).

**Finite domain and cluster formation.** Now suppose we have a finite domain  $x \in [-L, L]$  with either Neumann or periodic boundary conditions. The solution can be extended to an infinite domain by periodically extending  $\mu(x)$ . Then the density  $\rho(x)$  satisfies the same ODE (1.3a) and the same integral constraint (2.19), except that the density support  $a, b$  may collide with the domain boundary (if the domain is small enough), as  $d$  is increased. In other words the condition  $\rho(a) = 0$  in (2.19) is replaced by *either*  $\rho(a) = 0$  with  $a < L$  or  $a = L$ , and similarly, either  $\rho(b) = 0$  with  $b > -L$  or  $b = -L$ .

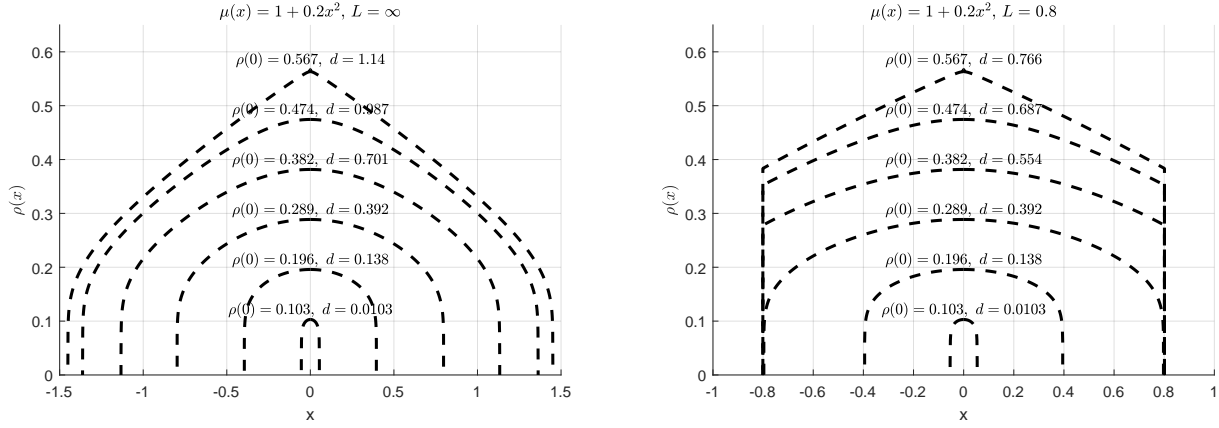


FIG. 3. Spike density  $\rho(x)$  for several values of  $d$  and with  $\mu(x) = 1 + 0.2x^2$ . Left: infinite domain  $L = \infty$ . Right: finite domain,  $L = 0.8$ . Note that in both cases, the maximum admissible value  $d_{\max}$  corresponds to  $\rho(0) = 1/\operatorname{arccosh}(3) = 0.567$ .

To illustrate, consider again the same  $\mu(x) = 1 + 0.2x^2$ , on a domain  $[-L, L]$  with  $L = 0.8$ . Recall that we found  $l_{\max} = 1.45 > L$ . This means that as  $d$  is gradually increased, the cluster *first* collides with the domain wall, and *then* the instability sets in. Let  $d_c$  denote the value of  $d$  when the cluster collides with the boundary. To find  $d_c$ , we solve the ODE (1.3a) with constraints (2.19) and an additional constraint that  $b = L$ . We find that  $d_c = 0.39$ . We then determine  $d_{\max} = 0.766 > d_c$ . As seen in Figure 2 (bottom left), both  $d_c$  and  $d_{\max}$  agree very well with full PDE simulations.

**Piecewise constant  $\mu$ .** An interesting special case is that of piecewise-constant  $\mu(x)$ . Here, we take the domain to be  $x \in [0, L]$  and take

$$\mu = \begin{cases} \mu_1, & 0 < x < l \\ \mu_2, & l < x < L \end{cases} \quad (2.22)$$

For the purpose of numerics, we use a smoothed-out step function for  $\mu(x)$ , namely:

$$\mu(x) = (\mu_1 - \mu_2) (0.5 - 0.5 \tanh(10(x - l))) + \mu_2. \quad (2.23)$$

From the ODE (1.3a) it follows that  $\rho(x)$  is also piecewise constant, with

$$\rho(x) = \begin{cases} \rho_1, & 0 < x < l \\ \rho_2, & l < x < L \end{cases} \quad (2.24)$$

where  $\rho_1, \rho_2$  satisfy

$$\int_{\rho_2}^{\rho_1} \frac{\cosh(1/\rho) - 3}{\rho^2 \sinh(1/\rho) (3\rho - \frac{5}{2} \sinh(1/\rho))} d\rho = \log\left(\frac{\mu_1}{\mu_2}\right), \quad (2.25)$$

whereas  $\int \rho = d$  yields

$$d = l\rho_1 + (L - l)\rho_2. \quad (2.26)$$

Let us assume that  $\mu_1 < \mu_2$  and as before, we must have  $0 < \rho_1, \rho_2 < \rho_{\max}$ . Since the integrand is negative on this range, it follows that  $\rho_1 > \rho_2$ , so that the spikes are more dense at the lower value of  $\mu$  – consistent with the physical interpretation of  $\mu$  being the decay rate of the activator.

Figure 4 shows the steady state with 10.5 spikes (10 spikes plus a half boundary spike at  $x = 0$ ). There, we took  $\mu_1 = 1, \mu_2 = 1.25$  with  $D = 0.005$  so that  $d = 0.74$ . Solving (2.25) subject to (2.26) yields  $\rho_1 = 0.48, \rho_2 = 0.27$ . The fraction of mass between 0 and  $l$  is then given by  $l\rho_1/d = 64\%$ , corresponding to 6.7 out of 10.5 spikes. This is in excellent agreement with Figure 4, where 6.5 spikes are located to the left of  $x = l$ .

It is possible that for a given choice of  $\rho_1 \in (0, \rho_{\max})$ , no (positive) solution for  $\rho_2$  to (2.25) exists. In this case we take  $\rho_2$  to be zero and a cluster forms on  $[-l, l]$ , *regardless* of  $L$ . Let  $\rho_c$  denote the *maximum* such  $\rho_1$ ; it satisfies

$$\int_0^{\rho_c} \frac{\cosh(1/\rho) - 3}{\rho^2 \sinh(1/\rho) (3\rho - \frac{5}{2} \sinh(1/\rho))} d\rho = \log\left(\frac{\mu_1}{\mu_2}\right). \quad (2.27)$$

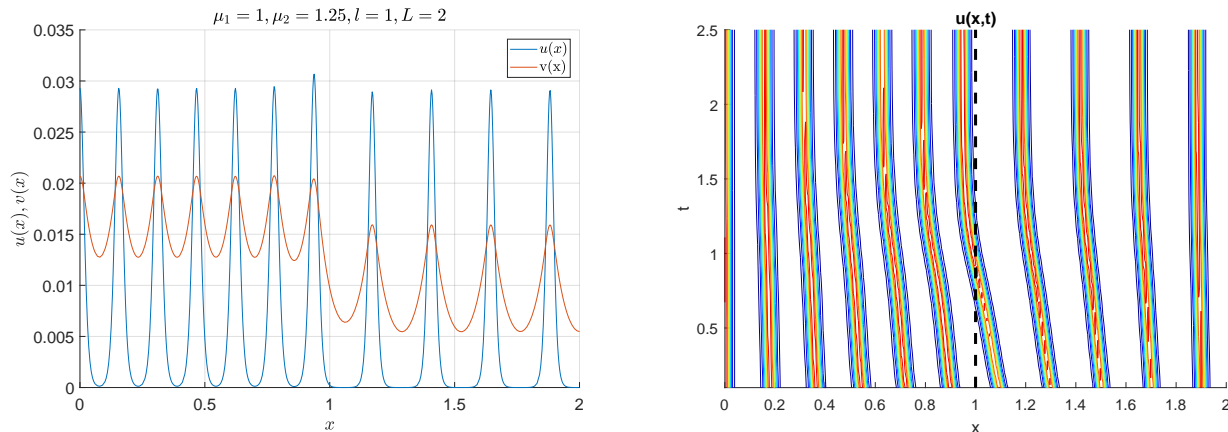


FIG. 4. Left: Steady state for piece-wise constant  $\mu(x)$ . The figure shows final steady state for the full PDE system (1.3a). Parameter values are:  $D = 0.005$ ,  $\varepsilon = 0.01$ ,  $x \in (0, L)$ ,  $\mu(x)$  as in (2.23) with  $\mu_1 = 1, \mu_2 = 1.25$ ,  $l = 1$  and  $L = 2$ . Theory predicts 64% of spikes inside  $[0, 1]$  and 36% of spikes inside  $[1, 2]$ , in excellent agreement with full numerics. Right: space-time plot of the transient dynamics. For initial conditions, 10.5 spikes uniformly distributed along  $[0, 2]$  were used.

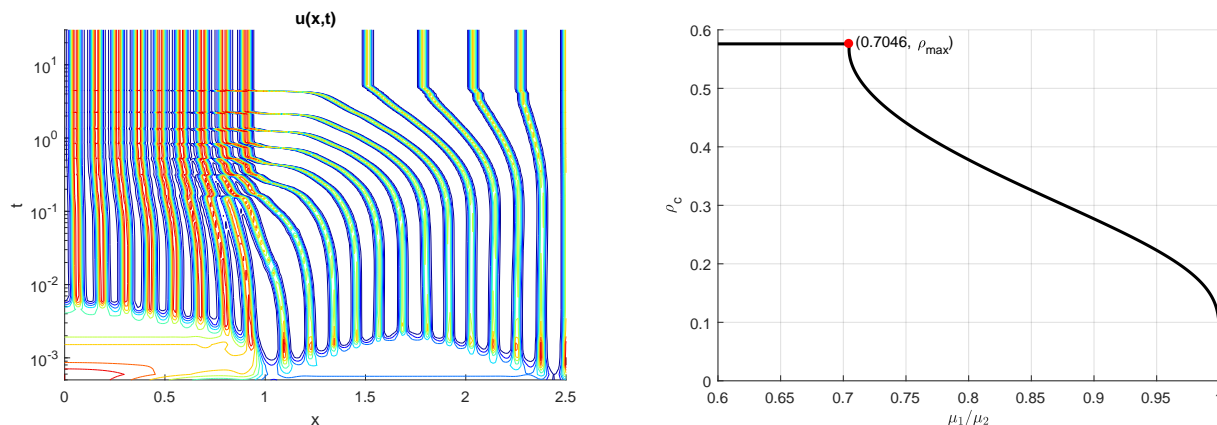


FIG. 5. Left: Space-time plot of the solution to (1.1) on the domain  $x \in [0, 2.5]$  with  $\mu(x)$  given by (2.23) with  $\mu_1 = 1, \mu_2 = 2$ ;  $\varepsilon = 0.01$ , and  $D = 0.00128$ . Two distinct clusters result after complex transient dynamics. Right: plot of  $\rho_c$  defined by (2.27) versus  $\mu_1/\mu_2$ .

Figure 5 (right) shows the plot of  $\rho_c \in [0, \rho_{\max}]$  as a function of the ratio  $\mu_1/\mu_2$ . Then for any  $\rho_1 \leq \rho_c$ ,  $\rho_2$  is taken to be zero. In this case, the density has a compact support  $[-l, l]$  regardless of  $L$ , corresponding to a spike cluster. Conversely, if  $\rho_1 > \rho_c$ , then the density is nonzero on  $[0, L]$  with  $\rho_2$  given by (2.25). From Figure 5(right), we see that when  $\mu_1/\mu_2 < 0.7046$ , we have  $\rho_2 = 0$  for all  $\rho_1 \in (0, \rho_{\max})$ . In this case, the spike cluster has compact support  $[0, l]$ ; and the instability threshold is given by  $d_{\max} = 2l\rho_{\max}$ .

In Figure 5 (left) we take  $\mu_1/\mu_2 = 0.5 < 0.7046$ , so that we expect the cluster to have a compact support  $[0, l]$ . However running the simulation, we observe some spikes to the right of  $x = l$ . This is due to exponentially weak interaction between the spikes which can drop below machine precision. In fact, the spikes interact on the  $O(\exp(-r/\sqrt{D}))$  where  $r$  is the inter-spike distance. In this example, the gap between the cluster and the spike to its right is around  $r = 0.7$  and  $D = 0.00128$  which gives  $\exp(-r/\sqrt{D}) \approx 3 \times 10^{-9}$  which presumably falls below the computational precision.

### 3. DISCUSSION

As we have shown (see Main Result 2.2), the maximum spike density is given by  $\rho_{\max}$ . From (1.3b), this implies that the minimum inter-spike distance is bounded from below by  $\min |x_j - x_{j-1}| \geq \frac{d}{N} \arccos(3)$ . In terms of the

original diffusion parameter  $D$ , we obtain

$$\min |x_j - x_{j-1}| \geq \sqrt{D} \arccos(3). \quad (3.28)$$

Intriguingly, this result is *independent* of the choice of precursor  $\mu(x)$ . In other words, *there is an intrinsic minimal spike distance that cannot be reduced by choosing a different precursor*.

Let us now come back to the case of constant  $\mu$  on a bounded domain  $[-L, L]$ , for which the instability threshold was first derived in [1] (see formula (4.65) there, reproduced as formula (1.2) in the present paper). In this, case  $|x_j - x_{j-1}| = 2L/N$  for all  $j$ , so that (1.2) becomes

$$L/N \geq \sqrt{D} \frac{\arccos(3)}{2} = 0.8814\sqrt{D}. \quad (3.29)$$

It is an elementary exercise to show that  $\frac{\arccos(3)}{2} = \log(1 + \sqrt{2}) = 0.8814$ ; as such, threshold (3.29) is *identical* to (1.2), which was derived by entirely different methods. So our analysis recovers previously known results in the case of constant  $\mu$ .

Recently, we studied a similar question for the Klausmeyer (or Schnakenberg) model of spotty vegetation with spatially-variable precipitation rate [8]. There, we also found instability thresholds. But unlike the GM model (1.1), the model in [8] did not have localized clusters of spikes: the spike density was found to be non-zero along the entire domain regardless of the choice of precipitation rate. In addition, the analysis in [8] required completely different techniques; the problem there was more “nonlocal”, and required a fully non-local analysis including the use of Euler-Maclaurin formula.

Another recent study of collective motion in PDE’s is [9]. There, we studied the Gross-Pitaevskii Equation used to model Bose-Einstein condensates and whose solutions consist of vortex-like structures [9–11]. For a two-dimensional trap, an asymptotic reduction for motion of vortex centers yields an interacting particle system [12–14], which in turn can be reformulated as a nonlocal PDE in the continuum limit of many vortices [15, 16]. While the analysis is quite different than the present paper, the end result is similar in spirit: one obtains instability thresholds which yields the maximum number of allowable vortices as a function of trap rotation rate and its chemical potential.

Generally speaking, looking at the limit of many localized structures (be it spikes, vortices, or other structures) can lead to exciting new challenges. Compared to a very large literature on behaviour of individual or finitely many spikes, there are still relatively few results about the *collective* behaviour of many spikes. This is a very promising avenue for further research with many problems still to be explored.

#### 4. APPENDIX: EQUATIONS OF MOTION

In this appendix we derive the equations of motion (1.4) starting with the PDE system (1.1),

$$\varepsilon^2 u_t = \varepsilon^2 u_{xx} - \mu(x)u + u^2/v, \quad 0 = \frac{d^2}{N^2} v_{xx} - v + \frac{u^2}{\varepsilon}. \quad (4.30)$$

Let  $x_k(t)$  denote the position of  $k$ -th spike. In the inner region near  $x_k$  we expand,

$$\begin{aligned} x &= x_k(t) + \varepsilon y, \quad \mu = \mu_k + \varepsilon y \mu'_k + \dots \\ u(x, t) &= U_0(y) + \varepsilon U_1(y) + \dots, \\ v(x, t) &= V_0(y) + \varepsilon V_1(y) + \dots, \end{aligned}$$

Then to leading order we have

$$0 = U_{0yy} - \mu_k U_0 + \frac{U_0^2}{V_0}, \quad 0 = V_{0yy} \quad (4.31)$$

and at the next order we obtain

$$-x'_k U_{0y} = U_{1yy} - \mu_k U_1 + 2 \frac{U_0 U_1}{V_0} - \frac{U_0^2}{V_0^2} V_1 - \mu'_k y U_0 \quad (4.32)$$

$$0 = V_{1yy} + U_0^2 \quad (4.33)$$

Then  $V_0$  is a constant and therefore  $U_0$  can be written as

$$U_0 = w(y\sqrt{\mu_k}) V_0 \mu_k \quad (4.34)$$

where  $w(z) = \frac{3}{2} \operatorname{sech}^2(z/2)$  is the homoclinic ground-state solution to  $w_{zz} - w + w^2 = 0$ .

In the outer region, we write

$$v \sim \sum_{j=1}^N S_j G(x, x_j) \quad (4.35)$$

where  $G$  is the Green's function solution to

$$\frac{d^2}{N^2} G_{xx} - G + \delta(x, y) = 0 \quad (4.36)$$

given, on an infinite domain, by

$$G(x, y) = \frac{N}{2d} e^{-|x-y|\frac{N}{d}}. \quad (4.37)$$

The weights  $S_k$  are computed as

$$S_k = \int_{x_{j-}}^{x_j^+} \frac{u^2(x)}{\varepsilon} dx \sim \int_{-\infty}^{\infty} (w(y\sqrt{\mu_k}) V_0 \mu_k)^2 dy.$$

Matching inner and outer region we obtain

$$V_0 \sim v_k$$

and using  $\int_{-\infty}^{\infty} w^2(z) dz = 6$ , we obtain

$$S_k \sim 6\mu_k^{3/2} v_k^2.$$

Finally we formulate the solvability condition to determine  $x_k$ . Multiplying (4.32) by  $U_{0y}$  and integrating by parts, we then obtain

$$-x'_k \int U_{0y}^2 = - \int U_{0y} \frac{U_0^2}{V_0^2} V_1 - \int \mu'_k y U_0 U_{0y} \quad (4.38)$$

We simplify

$$\int \mu'_k y U_0 U_{0y} \sim -\frac{\mu'_k}{2} \int U_0^2 = -3v_k^2 \mu_k^{3/2} \mu'_k; \quad (4.39)$$

and, using  $\int w^2 dz = 6/5$ ,

$$\int U_{0y}^2 \sim \int_{-\infty}^{\infty} \left( \frac{d}{dy} (w(y\sqrt{\mu_k}) V_0 \mu_k) \right)^2 dy \sim \mu_k^2 v_k^2 \frac{6}{5} \quad (4.40)$$

Finally, we compute

$$\int U_{0y} \frac{U_0^2}{V_0^2} V_1 = \frac{1}{V_0^2} \int \frac{U_0^3}{3} V_{1y} \sim -\frac{\langle v_x \rangle_k}{v_k^3} \int \frac{U_0^3}{3} dy \sim -\langle v_x \rangle_k \frac{12}{5} \mu_k^{5/2}, \quad (4.41)$$

where we used  $\int w^3 = \frac{36}{5}$ , and where  $\langle v_x \rangle_k$  denotes the average of the slopes in the outer regions for  $v(x)$ ,  $\langle v_x \rangle_k := \frac{v_x(x_k^+) + v_x(x_k^-)}{2}$ . We have

$$\begin{aligned} \langle v_x \rangle_k &= \sum_{j=1}^N S_j \langle G_x(x, x_j) \rangle_k \\ &= \sum_{j=1}^N S_j \frac{N^2}{2d^2} e^{-|x_k - x_j|\frac{N}{d}} \operatorname{sign}(x_j - x_k) \end{aligned}$$

Here,  $\operatorname{sign}(x - y)$  is taken to be zero when  $x = y$ .

Substituting (4.39-4.41) into (4.38) yields the system (1.4).

- [2] J. Wei, M. Winter, Stable spike clusters for the one-dimensional Gierer-Meinhardt system, Submitted.
- [3] A. Gierer, H. Meinhardt, A theory of biological pattern formation, *Kybernetik* 12 (1) (1972) 30–39.
- [4] J. D. Murray, *Mathematical Biology. II Spatial Models and Biomedical Applications* {Interdisciplinary Applied Mathematics V. 18}, Springer-Verlag New York Incorporated, 2001.
- [5] J. Wei, M. Winter, *Mathematical aspects of pattern formation in biological systems*, Vol. 189, Springer Science & Business Media, 2013.
- [6] J. Wei, M. Winter, On the gierer-meinhardt system with precursors, *Discr. Cont. Dyn. Systems*.
- [7] D. Iron, M. J. Ward, The dynamics of multispikes solutions to the one-dimensional gierer–meinhardt model, *SIAM Journal on Applied Mathematics* 62 (6) (2002) 1924–1951.
- [8] T. Kolokolnikov, J. Wei, Pattern formation in a reaction-diffusion system with space-dependent feed rate, *SIAM Review* 60 (3) (2018) 626–645.
- [9] S. Xie, P. G. Kevrekidis, T. Kolokolnikov, Multi-vortex crystal lattices in bose–einstein condensates with a rotating trap, *Proc. R. Soc. A* 474 (2213) (2018) 20170553.
- [10] J. Abo-Shaer, C. Raman, J. Vogels, W. Ketterle, Observation of vortex lattices in bose-einstein condensates, *Science* 292 (5516) (2001) 476–479.
- [11] M. H. Anderson, J. R. Ensher, M. R. Matthews, C. E. Wieman, E. A. Cornell, Observation of bose-einstein condensation in a dilute atomic vapor, *science* 269 (5221) (1995) 198–201.
- [12] E. Weinan, Dynamics of vortex liquids in ginzburg-landau theories with applications to superconductivity, *Physical Review B* 50 (2) (1994) 1126.
- [13] A. Aftalion, Q. Du, Vortices in a rotating bose-einstein condensate: Critical angular velocities and energy diagrams in the thomas-fermi regime, *Physical Review A* 64 (6) (2001) 063603.
- [14] D. Yan, R. Carretero-González, D. Frantzeskakis, P. Kevrekidis, N. Proukakis, D. Sporn, Exploring vortex dynamics in the presence of dissipation: Analytical and numerical results, *Physical Review A* 89 (4) (2014) 043613.
- [15] D. E. Sheehy, L. Radzihovsky, Vortex lattice inhomogeneity in spatially inhomogeneous superfluids, *Physical Review A* 70 (5) (2004) 051602.
- [16] T. Kolokolnikov, P. Kevrekidis, R. Carretero-González, A tale of two distributions: from few to many vortices in quasi-two-dimensional bose–einstein condensates, *Proc. R. Soc. A* 470 (2168) (2014) 20140048.